The Development and Validation of Simple Empirical Models of Impingement Cooling from Full Surface Heat Transfer Coefficient Distributions

David R.H. Gillespie, Changmin M. Son and Peter T. Ireland
Dept. of Engineering Science, University of Oxford
Parks Road, OX1 3PJ, UK

Geoffrey M. Dailey
Rolls Royce plc., Turbine Aerothermal
Moor Lane, Derby DE24 8BJ, UK

ABSTRACT

A simple heat transfer model of a cast passage impingement cooling system with film-cooling extraction is presented. This was derived from detailed local Nusselt number distributions on all surfaces of the system, measured in a large scale model using transient liquid crystal techniques. These data were averaged over physically sensible regions correlated to local flow conditions. An energy balance technique was use to calculate the convective efficiency. A second conventional 'plate insert' impingement passage has also been investigated. Local Nusselt number distributions on the target and impingement plates were used along with correlated data to predict the overall convective efficiency, and determine the sensitivity of the prediction to the data resolution. A reduced instrumentation heat transfer test using fast response gas thermocouples mounted at the inlet and exit planes of the test section, was used to assess the validity of the empirical models.

INTRODUCTION AND BACKGROUND

There have been many comprehensive studies of impingement cooling flow and heat transfer characteristics. **Florschuetz et al. (1981 etc.)** produced an extensive set of heat transfer correlations, and a robust flow model for impingement into a confined cooling passage, which has been the basis of industry plate impingement design codes. **Bunker and Metzger (1990)** first investigated leading edge impingement using transient tests, noting that close nozzle to internal apex spacings are desirable. **Lucas et al. (1992), Van Treuren et al. (1993)** investigated the effect of the impingement plate thermal boundary condition, and obtained high resolution data liquid crystal under a single confined jet and for in-line and staggered arrays respectively. These results showed the characteristic local heat transfer coefficient distributions, and the highly distorted impingement in the presence of crossflow. **Gillespie et al. (1996)** noted that much higher average levels of heat transfer can be obtained by shaping the impingement hole. More recently workers have investigated enhancing impingement heat transfer by employing extended surfaces, **Taslim et al. (2000)** and **Son et al. (2000)**. The latter has shown that by carefully positioning the extended surfaces, heat transfer may be enhanced without incurring major additional drop in pressure.

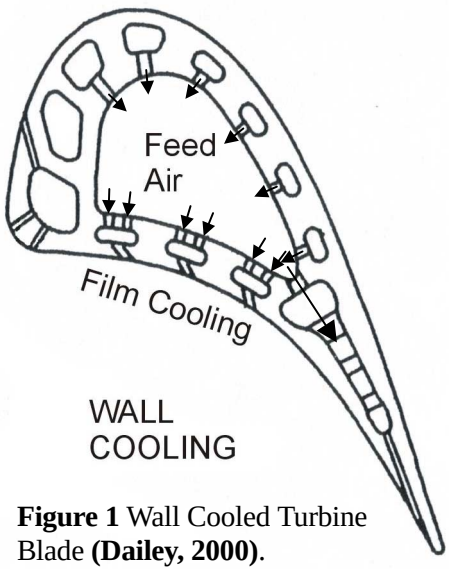

Figure 1 Wall Cooled Turbine Blade **(Dailey, 2000)**.

Previous workers have nearly always focused on heat transfer to the target plate. This was a sensible strategy while the impingement plate surface could not contribute to heat transfer from the hot outer surface of the blade. Recent improvements in casting technology mean that small passages may be integrally cast into the wall of the blade, **(Dailey, 2000)** *figure 1*. Such designs offer several thermal advantages: cooling airflow is restricted to the hot walls, there are reduced bend losses, and the pressure surface can be cooled using

Paper presented at the RTO AVT Symposium on "Advanced Flow Management: Part B – Heat Transfer and Cooling in Propulsion and Power Systems", held in Loen, Norway, 7-11 May 2001, and published in RTO-MP-069(I).

Report Documentation Page

Form Approved
OMB No. 0704-0188

1. REPORT DATE	2. REPORT TYPE	3. DATES COVERED
00 MAR 2003	**N/A**	**-**

4. TITLE AND SUBTITLE	5a. CONTRACT NUMBER
The Development and Validation of Simple Empirical Models of Impingement Cooling from Full Surface Heat Transfer Coefficient Distributions	5b. GRANT NUMBER
	5c. PROGRAM ELEMENT NUMBER
6. AUTHOR(S)	5d. PROJECT NUMBER
	5e. TASK NUMBER
	5f. WORK UNIT NUMBER
7. PERFORMING ORGANIZATION NAME(S) AND ADDRESS(ES) **NATO Research and Technology Organisation BP 25, 7 Rue Ancelle, F-92201 Neuilly-Sue-Seine Cedex, France**	8. PERFORMING ORGANIZATION REPORT NUMBER
9. SPONSORING/MONITORING AGENCY NAME(S) AND ADDRESS(ES)	10. SPONSOR/MONITOR'S ACRONYM(S)
	11. SPONSOR/MONITOR'S REPORT NUMBER(S)

12. DISTRIBUTION/AVAILABILITY STATEMENT
Approved for public release, distribution unlimited

13. SUPPLEMENTARY NOTES
Also see ADM001490, presented at RTO Applied Vehicle Technology Panel (AVT)Symposium held in Leon, Norway on 7-11 May 2001, The original document contains color images.

14. ABSTRACT

15. SUBJECT TERMS

16. SECURITY CLASSIFICATION OF:			17. LIMITATION OF ABSTRACT	18. NUMBER OF PAGES	19a. NAME OF RESPONSIBLE PERSON
a. REPORT	b. ABSTRACT	c. THIS PAGE			
unclassified	**unclassified**	**unclassified**	**UU**	**14**	

impingement. There is an obvious improvement in the thermal coupling between internal and external impingement surfaces, all of which now contribute to the external cooling. The associated improved structural integrity allows deployment of such impingement systems in rotating blades. While local data reported by the authors: **Gillespie et al. (1998)** and **Son et al. (2000, 2001)**, show how hot spots may be minimised for a particular cooling device, and how enhancement can be optimised, the engine designer requires correlations of average heat transfer coefficients to assess the overall performance of a proposed cooling geometry at blade operating conditions. They must also be able to compare different proposed cooling geometries. In this paper the local Nusselt number distributions characterised in a model of a prototype wall cooling geometry have been used to produce a correlation of average Nusselt number on the various surfaces of the passage. These have been sensibly split into areas of differing flow regimes to allow estimates of overall of Nusselt number to be made in slightly varying cooling geometries. The subsidiary heat transfer zones, i.e. those not on the target surface, were used along with averaged target surface data from a more conventional cooling configuration to model the overall heat transfer in such a passage. For both geometries it has been possible to calculate the convective efficiency at near engine operating conditions. The predictions of convective efficiency using measured and correlated data are in good agreement. These predictions were compared to thermocouple data taken during the transient heat transfer tests. Where careful experimental design meant that the experimental rig was engine representative throughout, remarkably good agreement was seen.

DERIVATION OF COOLING MODEL

The initial section of the paper explains the experiments carried out to determine the heat transfer coefficient correlations, and how these correlations were used to predict the overall convective efficiency of the cast passage cooling device.

Experimental Apparatus

The initial set of experiments were carried out in a model of a cast passage geometry with film-cooling extraction, typical of one novel blade cooling technique proposed by Rolls-Royce. A staggered double row of seven impingement holes exhausting through a single row of five inclined film cooling holes was chosen to represent part of an impingement passage. The impingement hole surface (equivalent to the impingement plate in conventional designs) has thickness to impingement hole diameter ratio, $\boldsymbol{l/d}$, equal to 1.25. This is the same as the space between the target plate and this holed surface, $\boldsymbol{z/d}$. The spanwise pitch of the impingement holes is $4\boldsymbol{d}$ and the array is offset from the spanwise passage centre line by $\pm 1.90\boldsymbol{d}$. The film-cooling holes are $1.08\boldsymbol{d}$ diameter, and pass through a $3.33\boldsymbol{d}$ thick target plate inclined to its surface at 30°. The spanwise pitch of these holes is $5.475\boldsymbol{d}$. The entrance and exit of the impingement holes are radiused ($\boldsymbol{R}0.45\boldsymbol{d}$ and $\boldsymbol{R}0.2\boldsymbol{d}$ respectively) to represent cast features, while the film-cooling holes are sharp edged to represent laser machined holes. Air enters the impingement holes from a fibre-board inlet plenum of dimensions $40\boldsymbol{d} \times 24\boldsymbol{d} \times 20\boldsymbol{d}$ and passes into a cavity $7.5\boldsymbol{d}$ wide, with radiused corners, *figure* 2. A perspex impingement plate was manufactured at 20:1

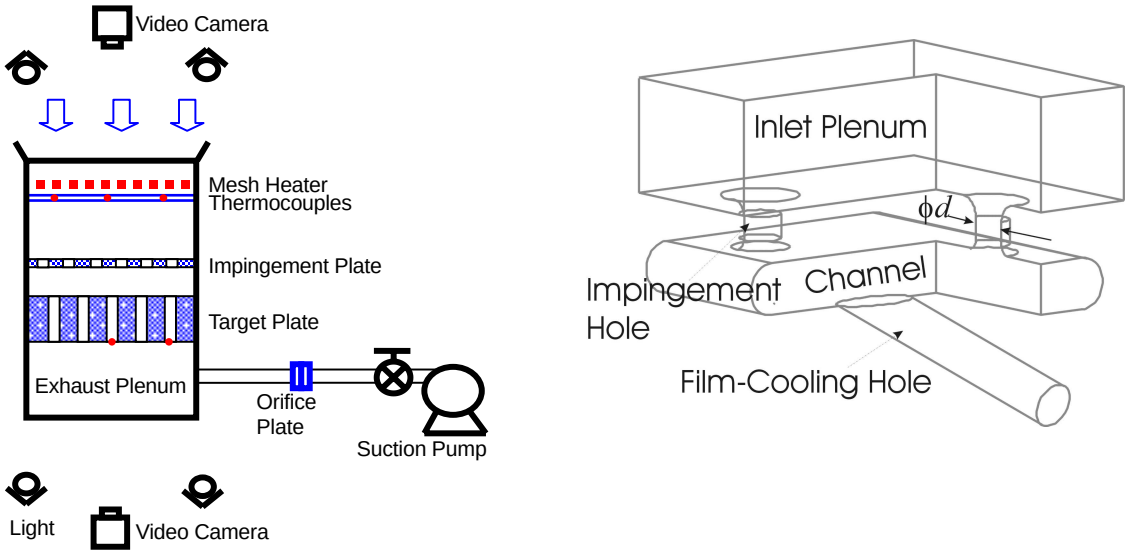

Figure 2 Schematic diagram of the test rig and details of the working section

scale model of an engine configuration. The target plate and cavity end walls were also manufactured from perspex. A compact planar heater[1] mounted across the inlet 15***d*** upstream of the working section provided a rapid, uniform increase in gas temperature at the start, and a steady gas temperature throughout the experiment. For full experimental details see **Gillespie et al. (1998)**. In all the experiments performed a coating of wide band thermochromic encapsulated liquid crystals applied to the model surface was used to measure the perspex surface temperature. The recorded video data was digitised at a frame rate of 50 frames per second and with a spatial resolution of approximately 3 pixels per millimetre on the model surface.

EXPERIMENTAL TECHNIQUE AND PREVIOUSLY REPORTED RESULTS

The full surface heat transfer coefficient distributions used to produce the first set of Nusselt number correlations were measured by **Gillespie et al. (1998)** using the transient liquid crystal technique. In cases when the local adiabatic temperature is known and a single crystal colour change event is recorded, it has been shown that the method yields h with an uncertainty of less than 7 percent **(Gillespie , 1996**). **Wang et al. (1994)** showed that a wide band colour liquid crystal technique, as used in this investigation, allows the method to be extended to obtain both h *and* T_{aw} with an uncertainty of 7.5 - 8.5% and 1.5 - 2.1% respectively. It is the uncertainty in the measured value of the thermal product of perspex, $\sqrt{\rho ck}$ = 569±29 $Ws^{½}/m^2K$ **(Ireland, 1987)**, and the 50 Hz video frame recording rate which predominately account for these uncertainties. Their technique used a full temperature history derived from the liquid crystal colour play. The techniques described above were developed and used by the present authors. Prior to the start of each test, the model temperature is uniform and equal to the room temperature. Air from atmosphere passes, unheated, through the rig and the mass flow rate is adjusted to obtain the desired jet Reynolds number. The experiment begins when electrical power is switched to the heating mesh. The mesh temperature then increases, with a first order lag, to a steady value determined by the air velocity, atmospheric temperature and flow speed. The time constant, τ, has been characterised by the authors. The gas transport time through the mesh is negligible and so the heated air temperature increases with the same time constant. Maximum test times were limited to approximately 60 seconds since this corresponds to the time taken for the thermal pulse to penetrate the thinnest section of the model wall **Schultz and Jones (1973)**. The mass flow rate remained steady throughout the test and the value determined from an average of continuously logged signal was used to calculate the average jet Reynolds number. The velocity through the heater mesh in impingement experiments is low (of order 10^{-2} ms^{-1}) and a step change in the power supplied does not cause the flow temperature to change as a step. The normal surface temperature response of the perspex substrate under a step change in fluid temperature is given by the familiar equation

$$T_{surface} = T_{init} + \left(T_{aw} - T_{init}\right) e^{\frac{h^2 t}{\rho ck}} \operatorname{erfc}\left(\frac{h\sqrt{t}}{\sqrt{\rho ck}}\right) \qquad (1)$$

When the heat transfer driving fluid temperature changes with a time constant, τ, the equation for the surface temperature rise becomes, **Gillespie (1996)**,

$$\frac{T_{surface} - T_{init}}{T_{aw} - T_{init}} = 1 - \frac{\frac{\rho ck}{h^2 \tau}}{\left(1 + \frac{\rho ck}{h^2 \tau}\right)} e^{\frac{h^2 t}{\rho ck}} \times \operatorname{erfc}\left(\frac{h\sqrt{t}}{\sqrt{\rho ck}}\right) - e^{-\frac{t}{\tau}} \frac{1}{\left(1 + \frac{\rho ck}{h^2 \tau}\right)} \times \left(1 + \frac{\sqrt{\rho ck}}{h\sqrt{\tau}}\left(\frac{1}{\pi}\sqrt{\frac{t}{\tau}} + \frac{2}{\pi}\sum_{1}^{\infty}\frac{1}{n} e^{-\frac{n^2}{4}} \sinh n\sqrt{\frac{t}{\tau}}\right)\right) \qquad (2)$$

The heat transfer coefficient and the driving gas temperature difference are then chosen to obtain the best fit between the experimental data and the analytical model of equation (2), *figure 3*. Local maps of Nusselt number on both the target surface and impingement surfaces are shown in *figure 4*.

Average Values

The Nusselt number at conditions other than those measured may be estimated by correlating Nusselt number to Reynolds number on each of the heat transfer surfaces. To help allow the results to be used further to estimate the heat transfer in devices with slight changes in geometry, the surfaces have been sub-divided into regions of enhanced and unenhanced heat transfer. Distinct changes in the heat transfer levels, and the results

[1] UK Patent PCT/GB96/2017.

of Oil of Wintergreen / TiO_2 flow visualisation, *figure 5*, were used to determine the boundaries of these regions.

On the upstream surface of the impingement plate the area of enhancement around each impingement hole has been represented by a strip of area $\pm x_h/2$ by ($y_h/2$ + $d/2$) between the passage centreline and the outside edge of the impingement hole, the rest of the area lying outside the zigzag strip of heat transfer enhancement. The enhancement is linked to the thickness of the developing boundary layer on this surface. The effect of adding extra holes would be to add additional enhanced patches to this surface. The pattern of heat transfer coefficient in this area is not likely to be representative, as in most engine cooling systems there will be significant crossflow. It is necessary to accurately model all heat transfer surfaces in order to assess the model's accuracy in the analysis set out below. In the impingement hole, it was necessary only to consider the straight-sided portion of the hole. Notably on these surfaces the Nusselt number scales with $Re_{jet}^{½}$, suggesting that in these regions the flow remains laminar. The whole of the downstream face of the impingement plate, showing no distinct areas of heat transfer enhancement, has been considered as a single heat transfer surface, which scales with $Re_{jet}^{1.07}$. On the target surface, the results of flow visualisation showed that 83% the flow lay in the wall jet region, while 17% lay outside this region, and the Nusselt number correlation has been determined accordingly which scales with $Re_{jet}^{1.10}$. While the Nusselt number dependency on the down stream face of the impingement plate and in the portion of the target surface outside the wall jet lies between 0.7 and 0.8, which is typical of turbulent flow, in the wall jet region the dependence is surprisingly high at $Re_{jet}^{1.11}$. This can be explained by the large increases in heat transfer coefficient in the portion of the wall jet which undergoes transition to a turbulent regime as the jet Reynolds number is increased. The area covered by this region of the wall jet is large compared to the region of peak heat transfer coefficient near the centre of the jet. The dependence is not dissimilar to that of **Van Treuren et al. (1996)** who found that in the wall jet region of a staggered array of impinging jets in

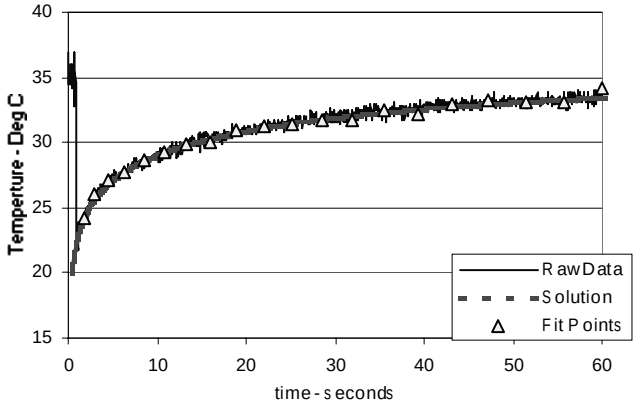

Figure 3 Typical fit of hue based temperature measurements to analytical model of heat transfer

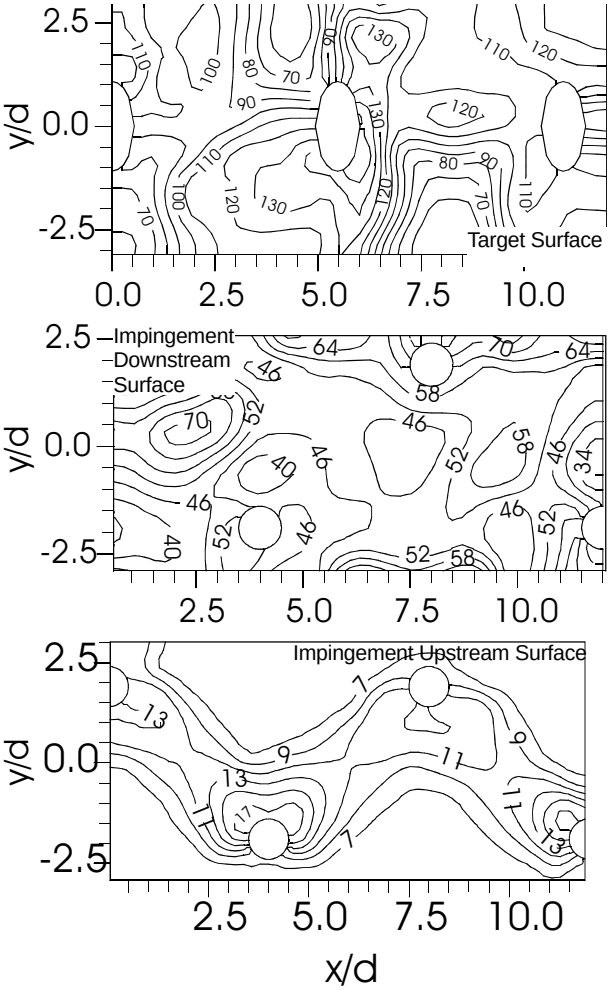

Figure 4 Local Nusselt Number Data $Re_{jet} \approx 41{,}000$

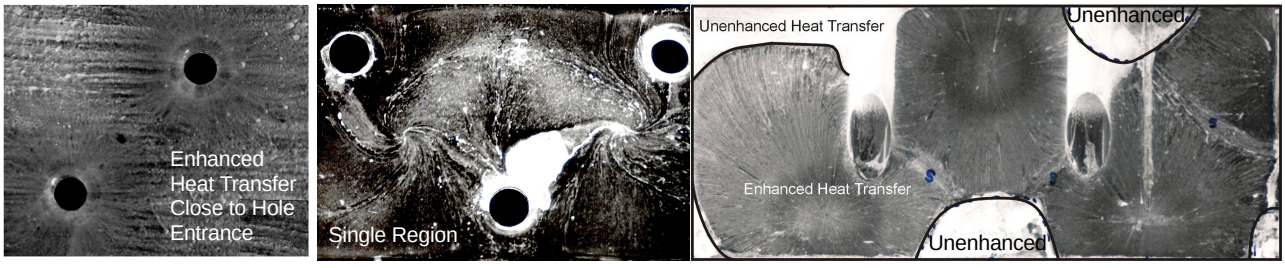

Figure 5 TiO_2 / Oil of Wintergreen flow visualisation on the upstream and downstream sides of the impingement plate and the target plate respectively.

crossflow $\boldsymbol{Nu} \propto \boldsymbol{Re_{jet}}^{0.923}$. The average heat transfer coefficient on each surface determined from the experimental data are shown in *table 1*. The final column of the table approximately shows the contribution of each heat transfer surface to the overall heat transferred between the blade and the coolant at $\boldsymbol{Re_{jet}}$ = 41170.

Surface	Heat Transfer Coefficient W/m^{2}K, $\boldsymbol{Re_{jet}}$ =41170	$\boldsymbol{Re_{jet}}^{\boldsymbol{n}}$ $\boldsymbol{n}$	Area (Symbolic)	$\frac{\bar{h}A}{\sum \bar{h}A}$ % $\boldsymbol{Re_{jet}}$ =41170
Upstream Impingement Plate (Enhanced)	32.53	0.5	$\boldsymbol{x_h}\,(\boldsymbol{y_h}/2+\boldsymbol{d}/2) - \pi\boldsymbol{d}^2/4$	2.98
Upstream Impingement Plate (Unenhanced)	18.75	0.5	$\boldsymbol{x_h w} - \boldsymbol{x_h}\,(\boldsymbol{y_h}/2+\boldsymbol{d}/2)$	
Impingement Hole	35.79	0.5	$0.071\,\pi\boldsymbol{d}$	0.36
Downstream Impingement Plate	124.2	0.696	$\boldsymbol{x_h w} - \pi\boldsymbol{d}^2/4$	16.8
Concave Cavity Walls	234.4	1.07	$2[\boldsymbol{x_h}\,(\pi\boldsymbol{d}_{endwall}/2)]$	14.7
Target Plate (Wall Jet, Enhanced)	321.5	1.11	$0.83\,\boldsymbol{x_h w}$	41.1
Target Plate (Unenhanced)	158.9	0.787	$0.17\,\boldsymbol{x_h w}$	
Film-Cooling Hole	259.3	0.8	$[\boldsymbol{x}_{h\ impingement}/\boldsymbol{x}_{h\ f\text{-}c}]\,.\,\pi\boldsymbol{d}_{h\ f\text{-}c}\,\boldsymbol{l}_{h\ f\text{-}c}$	24.1

Table 1 Heat Transfer Data

Simple Model of Wall Cooling Convective Efficiency

The calculated convective efficiency (equation 3) of a 'standard blade' **(Halls, 1969)** of infinite conductivity cooled using the candidate geometry can be used by the designer to rank overall performance. It is particularly useful to quickly estimate the change in steady state blade temperature using the measured heat transfer coefficients.

$$\eta = \frac{T_{g\,exit} - T_{gin}}{T_w - T_{gin}} \tag{3}$$

First an energy balance is applied between the heat transferred to the blade along the cooling passage, and the change in enthalpy of the coolant. Here, the impingement passage and film-cooling holes must be considered as two coupled cooling devices, with the gas exit temperature from the impingement passage being the inlet temperature of the film-cooling holes. Inside the cooling cavity a single driving gas temperature has sensibly been assumed as the coolant is highly mixed and the coolant path length is low.

$$\dot{m}c_p dT_g = \sum h_i \left(\frac{A_i}{l}\right)\left(T_w - T_g\right) \mathrm{d}l\,, \tag{4}$$

where h_i = heat transfer coefficient on each region, A_i = surface area of each region, and l = the coolant path. Integration of equation (4) and substitution into equation (3) yields the relationship between convective efficiency and the heat transfer coefficients measured and correlated above:

$$\eta_{impingement\ cavity} = \frac{T_{g\,cavity\,exit} - T_{gin}}{T_w - T_{gin}} = 1 - \mathrm{e}^{-\sum_{i=1}^{n} \frac{h_i A_i}{\dot{m}c_p}}\,. \tag{5}$$

This procedure is repeated for the film-cooling hole. Furthermore, it can be shown that the convective efficiency of the coupled system can then be written as:

$$\eta = \frac{T_{g\,exit} - T_{gin}}{T_w - T_{gin}} = \eta_{impingement\ cavity} + \eta_{film\text{-}cooling\ hole} - \eta_{impingement\ cavity} \times \eta_{film\text{-}cooling\ hole} \text{ (Suo, 1985).} \tag{6}$$

The system convective efficiency reported takes no account of the film-cooling on the external blade surface. The average Nusselt number inside the film-cooling holes is determined by the Dittus-Boelter correlation for fully developed turbulent flow. **Gillespie et al. (1996)** observed very greatly reduced enhancement at the entrance of both normal and inclined film-cooling holes in the presence of crossflow: thus no enhancement has been applied to account for the holes' small ***l/d***. The estimate of convective efficiency made using the correlated values of heat transfer coefficient is shown on *figure 6*. The convective efficiency has been determined for a representative spanwise passage width of one impingement hole pitch. The contribution of each surface to the overall cooling performance are given in the final column of *table 1*; values are presented relative to those at the impingement target surface, i.e. what could be obtained using a conventional plate insert impingement configuration. No attempt has been made to account for the changing wall temperature of the cooling passage in the real engine environment, though this will tend to reduce the enhancement of heat transfer. This technique is particularly useful where it is only possible to make the experimental rig engine representative in a small portion of the working section.

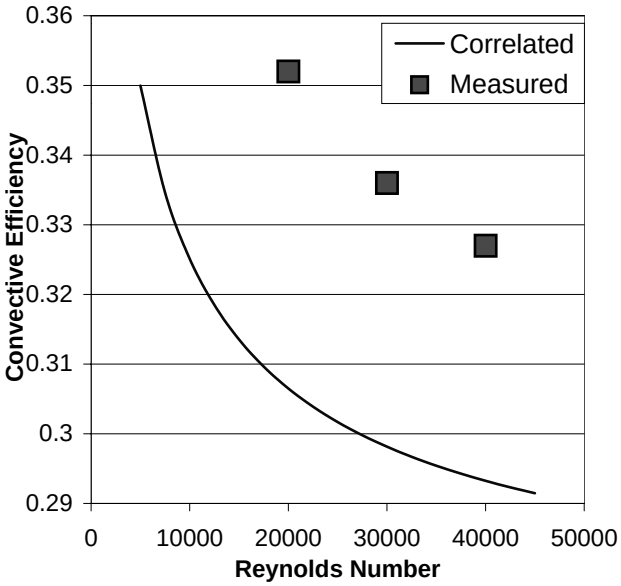

Figure 6 Convective Efficiency of Cast Passage Cooling Device

As a comparison, the convective efficiency of the test rig was measured directly using fast-response thermocouples located in the inlet plenum and at the centreline exit of the film-cooling holes. A dimensionless temperature determined at the start of the test (defined in a way very similar to convective efficiency) was used to calculate an effective uniform model wall temperature. At the start of the test, where the model wall temperature is the initial temperature everywhere, the dimensionless centreline exit temperature, ξ, defined below was determined.

$$\xi = \frac{T_{in} - T_{cl\,exit}(0)}{T_{in} - T_w (= T_{init})} \tag{7}$$

In fact if the mixed bulk temperature were used for the inlet and exit temperatures, this group would correspond to the convective efficiency. As the temperature profile is reasonably flat for these experiments the centreline temperature is a close approximation to the mixed bulk temperature. An analysis of the boundary layer development on a flat plate implies that for a hole of ***l/d*** = 6.15, with no crossflow at the hole entrance, the flow at the exit is not fully developed and the boundary layer is less than 0.198***d*** thick. Here it has been assumed that:

$$\text{Momentum thickness} = 0.036\, x\, Re_x^{-0.2} \quad \textbf{(Kays and Crawford, 1980)}. \tag{8}$$

The relationship between the mixed bulk temperature and the centreline temperature can be found by integrating the product of velocity and temperature in the direction of the flow. Here it is necessary to use Reynolds' analogy within the boundary layer, and a turbulent profile has sensibly been assumed:

$$\frac{u}{U_\infty} = \left(\frac{T - T_w}{T_\infty - T_w}\right) = \left(\frac{y}{\delta}\right)^{1/7} \tag{9},$$

which leads to

$$T_{mb} - T_w = \frac{\int_0^A u(T - T_w)\,dA}{\int_0^A u\,dA}. \tag{10}$$

For the current series of tests T_{mb} - T_w = 0.926 (T_{cl} – T_w). This relationship was used to obtain the convective efficiency from ξ. The convective efficiency at each Reynolds number was calculated from logged thermocouple data, as shown in *figure 7* at Re_{jet} = 31200. A correction has been applied to the exit centreline thermocouple signal to account for its finite time response, and this is shown in the figure. Further evidence of the uniformity of the film-cooling exit temperature profile was obtained by measuring the temperature distribution using a high porosity nylon mesh coated with wide band liquid crystal. **Gillespie (1993)** first measured the time response of a stainless steel mesh heater by coating the filaments with liquid crystal. **Wang et al. (1996)** developed this technique using a nylon mesh. Most recently the technique was used by **Mee et al. (1998)**, and **Gillespie and Ireland (1999)** to characterise the trajectories of coolant films. Their methods were employed in the current study, this limited additional pressure drop through the working section to 0.08 dynamic heads of the flow through the cooling holes. Film-cooling hole exit temperature distributions at time = 5, 10, 30 and 60 seconds, Re_{jet} = 31,200 are presented in *figure 8*. The surface is elliptical as the hole exits at 30 degrees to the surface. The non-uniformity seen in the bottom left hand quadrant of each surface plot is caused by the stem of the gas exit thermocouple. The position of each data point was determined by its video pixel location. Although regularly spaced, the grid points were not entirely symmetrical about the hole axis. This has caused noticeable discrepancies in the interpolated gas temperature around the edge of the hole, where the temperature gradients are highest. These are thought not to be due to any physical phenomenon.

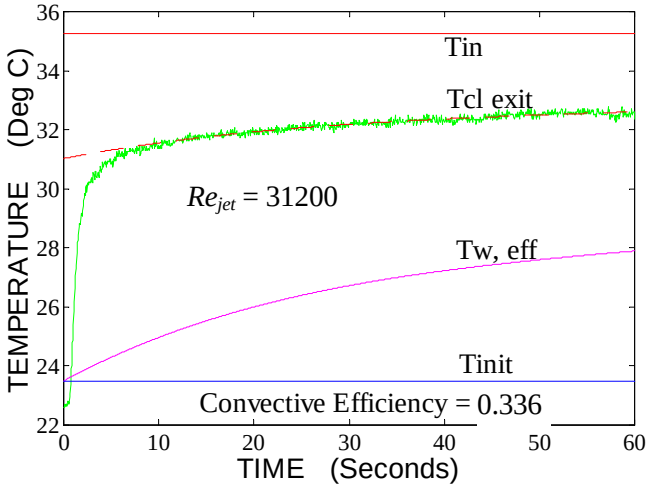

Figure 7 Logged thermocouple data used to directly measure the convective efficiency of the experimental rig

In a transient test it is only at the start of the experiment that the wall temperature is known. The value of the dimensionless temperature determined at the start of the test may be used to determine an effective uniform wall temperature throughout the test. The measured exit temperature distribution can then be rendered dimensionless, and may be compared to the convective efficiency. The mass flow rate weighted average of the non-dimensional exit temperature distribution is approximately equal to one minus the convective efficiency.

$$\frac{\theta(t)}{\theta_0} = \frac{T(x,y,t) - T_{w,eff}(t)}{T_{in} - T_{w,eff}(t)} \qquad (11), \qquad \text{where} \quad T_{w,eff}(t) = T_{in} - \frac{T_{in} - T_{cl\,exit}}{\xi} \qquad (12).$$

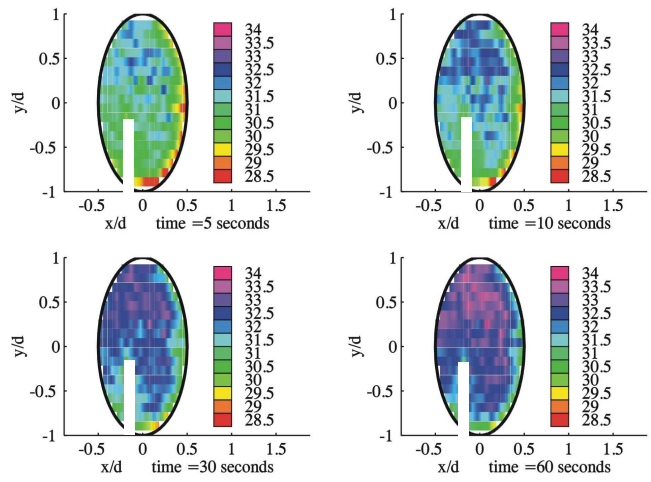

Figure 8 Film-cooling hole exit temperature profiles Re_{jet} = 31200.

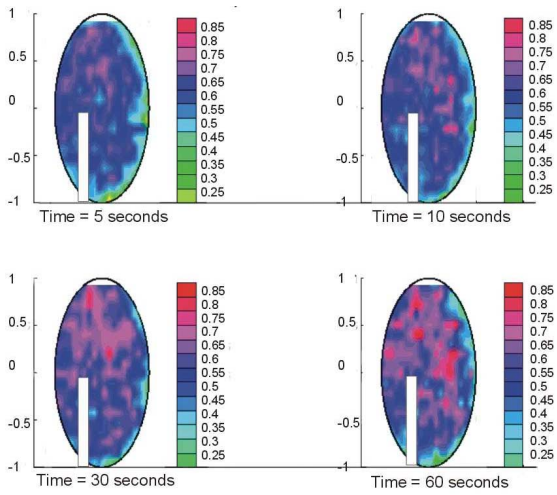

Figure 9 Film-cooling hole exit non-dimensional temperature profiles, Re_{jet} = 31200.

These non-dimensional exit temperature distributions are shown in *figure 9.* The unchanging level of the non-dimensional temperature during the first 30 seconds of the test is a good indication that the assumed conditions of a constant heat transfer coefficient distribution and a semi-infinite substrate pertain during this period.

The convective efficiency data determined from the thermocouple signals are shown on *figure 6.* The previous method calculated the convective efficiency of an engine representative section of the working section, but here the entire experimental facility is considered. This included the full extent of the inlet plenum, and an area of low velocity flow in each of the closed ends of the cooling cavity, which had a high residence time in the rig. As a result, for a given flow rate, the directly measured convective efficiency is slightly higher. However, in spite of these drawbacks, is should be noted that the technique is quickly implemented, and requires no knowledge of the local heat transfer data.

VALIDATION OF COOLING MODEL

Experimental Geometry

A second study has extensively investigated the heat transfer and flow characteristics of an existing turbine internal cooling system modelling a section of a nozzle guide vane, and a similar geometry with a uniform array of impingement holes. The particular impingement geometries are summarised in table 2, which includes a diagram clarifying the nomenclature. Both systems have a staggered array of impingement holes arranged in 2 / 3 columns (spanwise) and 6 rows (streamwise). The spent air exits from the chordwise downstream edge of the impingement channel. Odd and even rows contain 2 and 3 impingement holes respectively.

	Parameter	x_h/d	y_h/d	z/d	l/d
Uniform	Row 1-6	3.7	4.6	2.3	0.92
Non-Uniform	Row 1-3	4.8	6.0	3.0	1.2
	row 4-5	3.61	4.51	2.26	0.90
	row 6	3.00	3.75	1.88	0.75

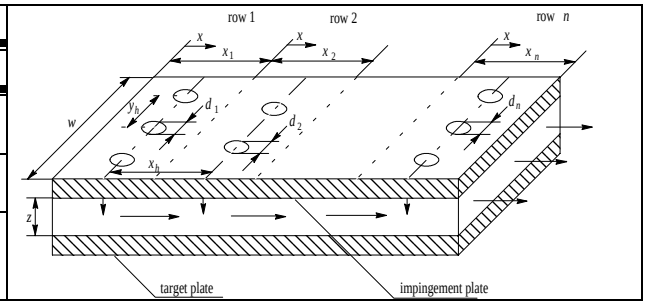

Table 2 Geometric Parameters of the Impingement Channel Validation Models

Test Rig and Heat Transfer Coefficient Measurements

The perspex test rig and its operation is fully described by **Son et al. (2000)**, for reference a cut away photograph is included as *figure* 10. The operation of the test rig is very similar to the rig described above. However, while all of the flow enters the cooling channel through the impingement holes as before; in this configuration air exhausts through the channel on one side only into an exit plenum. This means that there is increasing crossflow in the channel beneath each row of impingement holes. The impingement holes are of diameter 10 - 16 mm (***d*** = 13.3mm for the uniform array) and model engine conditions at approximately 20 times engine scale. Tests were carried out over a wide range of average jet Reynolds number, $\boldsymbol{Re_{jet}}$ = 15,000 - 40,000. The local heat transfer coefficient distributions were measured using a coating of three narrow band liquid crystals, to record single temperature events at 30°C, 34.5°C and 37.5°C not only to the target surface, but also to the impingement plate downstream surface, where there can be considerable heat transfer. During transient heat transfer experiments, 5 pressure signals and 12 thermocouple signals are monitored using an 8 channel A/D converter card and a 32 channel multiplexer installed in a PC. The typical sampling rate is 20 Hz and approximately 1500 data points per each channel are acquired in each test. Gas thermocouples were mounted immediately downstream of the heater mesh, and at the exit of the impingement channel, these were used to infer the cooling effectiveness of the test rig.

Typical local Nusselt number distributions on both the target plate and the uniform impingement plate downstream surfaces are shown in *figure 11.* The distortion of the circular impingement region by the increasing channel crossflow is clearly visible on the target surface, as are regions of low heat transfer between jets where the flow separates from the surface. On the impingement surface the structure is less clear, however, **Son et al. (2001)** show early in the passage regions of high heat transfer can be explained exclusively by the reimpingement of flow from the separation regions of the target plate. Nearer the exit of the test section, where

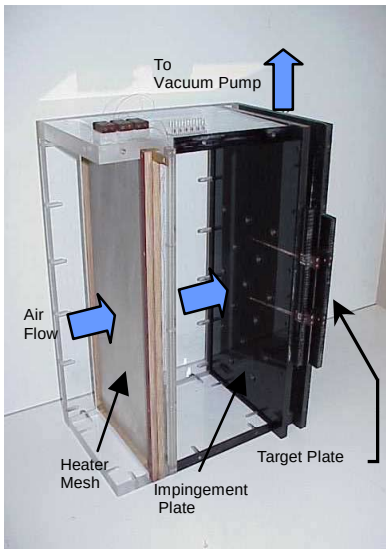

Figure 10 Test Rig Working Section

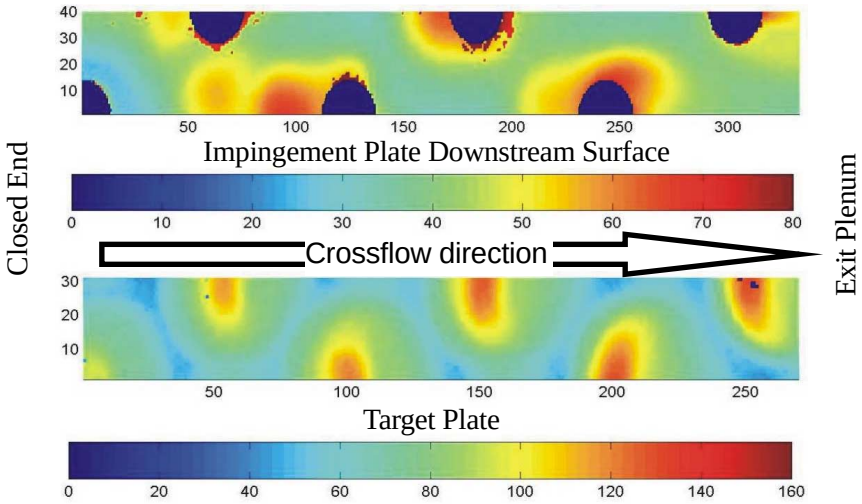

Figure 11 Nusselt number distributions on the downstream impingement and target plates respectively, uniform array.

the crossflow is more pronounced, enhancement is produced not only by reimpingement, but by interaction of the crossflow with the impinging jets which act like obstacles to the flow.

Energy Balance Techniques

A wide range of experiments has been carried out on this cooling geometry to optimise heat transfer to the target surface of the impingement channel, see **Son et al. (2000, 2001)**. Only limited data has been collected on heat transfer to the impingement plate downstream surface and none to the remaining wetted surfaces. These include the upstream impingement surface, impingement holes, side and end walls. It was speculated that these subsidiary areas of heat transfer would not strongly depend on the impingement geometry, and the correlations determined above were used to estimate the heat transfer coefficients in these regions. It is useful to be able to compare the convective efficiency of the entire cooling device to other systems, in order to do this a method was developed to account for the multiple coolant streams from successive rows of impingement holes. The impingement channel is considered as an isothermal surface, divided into streamwise sections half a pitch upstream and downstream of each impingement hole, *figure 12*.

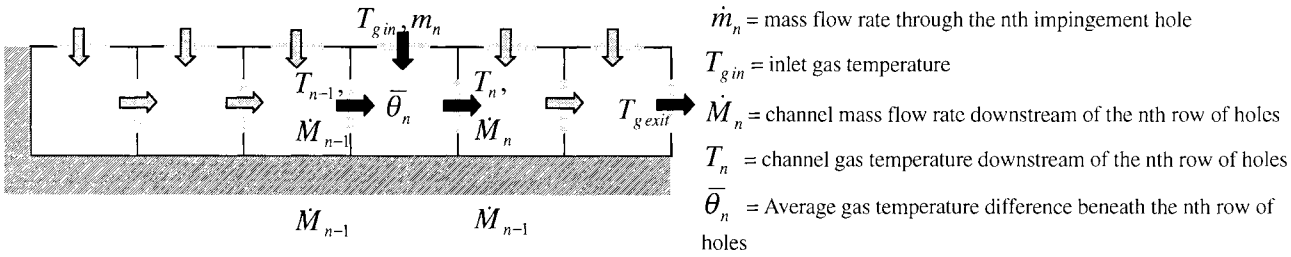

Figure 12 Mixing Box approach to obtain equivalent convective efficiency

At, for example the *nth* row of holes, the average inlet driving gas temperature difference, $\bar{\theta}_n$, is taken as the mass flow rate weighted average of the impinging flow and the incoming channel flow temperatures:

$$\bar{\theta}_n = \left(\frac{\dot{M}_{n-1}}{\dot{M}_n}\theta_{n-1} + \frac{\dot{m}_n}{\dot{M}_n}\theta_0 \right) \qquad \text{where } \theta_n = T_n - T_w,\ \theta_0 = T_{g\,in} - T_w . \tag{13}$$

A continuous injection model, where discrete injection at rows of impinging jets is distributed over the full impingement plate, was employed to obtain the mass flow rate distribution in the channel **Florschuetz et al.**

(1981). Again equating the change in enthalpy of the flow to the heat transferred to the wetted surfaces, equation (4), it can be shown that:

$$\theta_n = \left(\frac{\dot{M}_{n-1}}{\dot{M}_n} \bar{\theta}_n + \frac{\dot{m}_n}{\dot{M}_n} \theta_0 \right) e^{-\sum \frac{h_i A_i}{\dot{M}_n c_p}}. \tag{14}$$

The convective efficiency of the initial row, and hence θ_0, is given by equation (5). Thus the at exit row, N, the equivalent convective efficiency can be found:

$$\eta_N = \frac{T_{g\,exit} - T_{g\,in}}{T_w - T_{g\,in}} = 1 - \frac{\theta_N}{\theta_0}. \tag{15}$$

The convective efficiency of the impingement channel with each of the impingement plates installed was calculated at an average jet Reynolds number of $\boldsymbol{Re_{jet}}$ = 31047 with the uniform impingement plate and $\boldsymbol{Re_{jet}}$ = 30114 for the non-uniform array. These are shown along with the convective efficiency truncated to the exit of each row in *figure 13*. In the case of the non-uniform array it is clear that adding additional mass flow through larger holes in the downstream portion of the array acts to reduce the overall convective efficiency, although the final value is very similar for both geometries: $\boldsymbol{\eta}$ = 0. 173 and $\boldsymbol{\eta}$ = 0.168 for the uniform and non-uniform array respectively. This is notably lower than the level obtained in the cast passage geometry with film-cooling extraction. This is partly due to heat transfer in the film-cooling hole, the absence of which would reduce $\boldsymbol{\eta}$ to 0.247. However the main reason for the reduction in $\boldsymbol{\eta}$ is the greater mass flow rate in the confined cooling channel. The assumption that the correlated heat transfer coefficients on the minor heat transfer surfaces would adequately model the system performance is also borne out, producing a underestimation of the convective efficiency of 1.81% and 2.66% in the uniform and non-uniform cases respectively. These are within the limits of experimental error, as set out above.

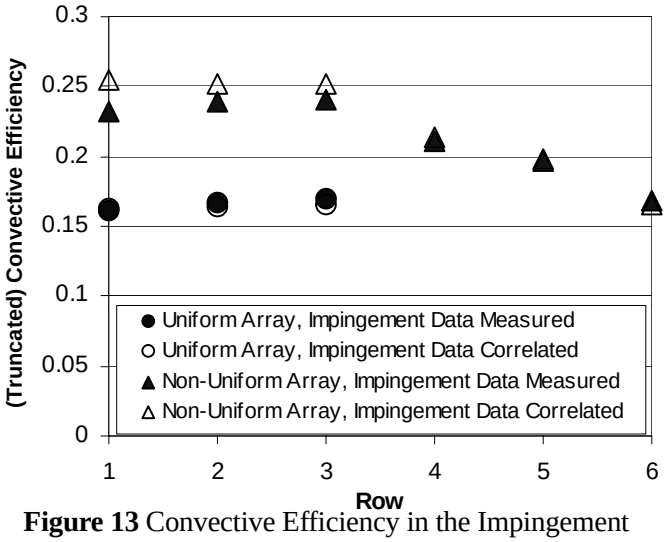

Figure 13 Convective Efficiency in the Impingement Cooling Array

Using a similar energy balance technique the overall change in enthalpy in each impingement row was calculated for each test case. The calculated exit gas temperature at time = 0 was compared to the measured gas temperature at the exit of impingement cooling channel. These are shown in *figure 14*. This provided a check as to the validity of the heat transfer coefficients assigned to the unmeasured surfaces. The calculation showed good agreement between the measured ($\boldsymbol{T_{exit\ measured}}$) and calculated ($\boldsymbol{T_{exit,}}$ row 6) exit gas temperature with a maximum difference of 2.5°C in the case of the uniform array and 0.5°C for the non-uniform array. *Figure 15* shows distribution of heat flow through the different heat transfer surfaces at each row. For the first row, heat flow rate through the end wall was included. In all cases the contribution of the target plate is the most significant contribution, while heat flow to the impingement plate, which may be in good thermal contact with the blade surface, lies at approximately 50% of this level.

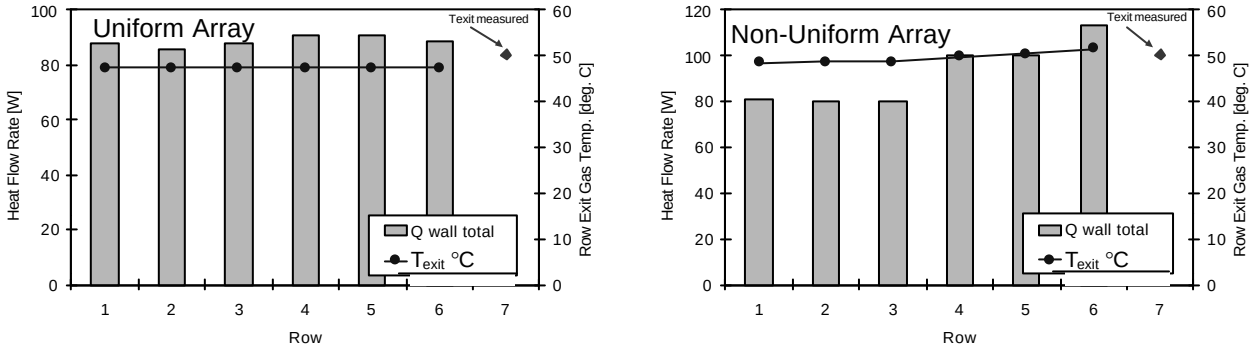

Figure 14 Total heat flow to the cooling passage, and inferred change in the channel gas temperature

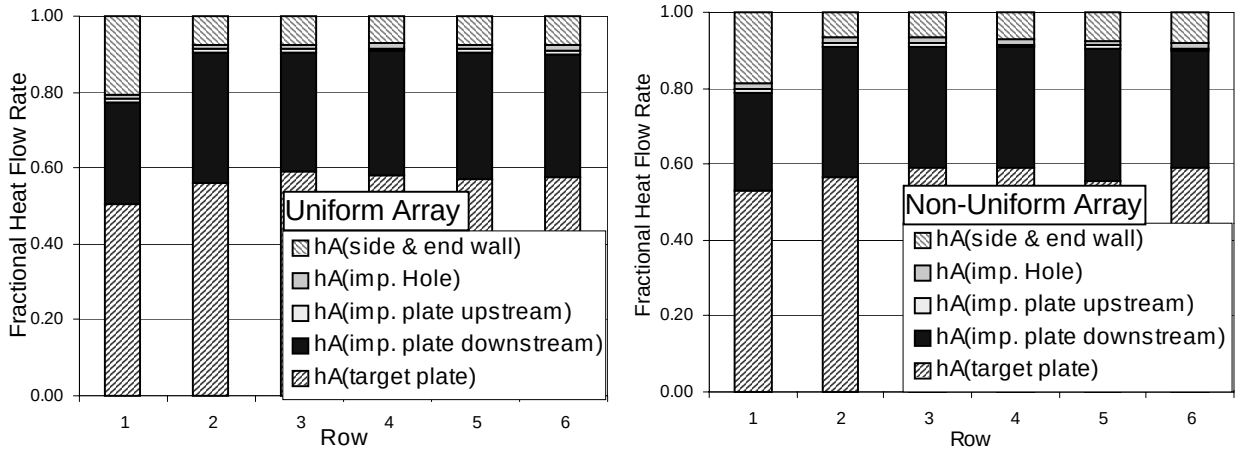

Figure 15 Fractional Heat Flow Rate through each portion of the channel

SUMMARY

A correlation of Nusselt number to average jet Reynolds number on all surfaces of a cast passage impingement channel was determined from detailed heat transfer coefficient measurements. It was postulated that heat transfer to surfaces other than the target surface is a weak function of the local cooling geometry. The correlation was shown to accurately predict the performance of other impingement cooling devices where only average data on the target surface was available, leading to a fast route for the assessment of impingement cooling geometries cast into the blade wall. It was also shown that the overall convective efficiency could be estimated for a system with multiple sources of coolant, and that in a well designed experimental facility this could be directly measured from appropriately sited thermocouples in a single transient test.

ACKNOWLEDGMENTS

The authors gratefully acknowledge the support of the Rolls-Royce plc, DERA, DTI CARAD and MOD ARP26c for the work reported here. The experimental apparatus was built by Mr P.J. Timms whose technical expertise is much appreciated.

NOMENCLATURE

A	area, m^2
c_p	specific heat capacity at constant pressure, J/kgK
d	hole diameter, m
erfc( )	1-erf( )
h	heat transfer coefficient, W/m^2K
k	thermal conductivity, W/mK
l	length, m
$\dot{m}$	
$\dot{M}$	mass flow rate along channel, kg/s
Nu	Nusselt number = hd/k
q	heat flux, W/m^2
Re_{jet}	Average jet Reynolds number, $\frac{4\dot{m}_h}{\pi d\mu}$
t	time, s
T	temperature, °C
U,u	velocity, ms^{-1}
w	channel width, m
x,y	distance from the working section origin, m
y	height in boundary layer, m
z	distance from the impingement plate to the target plate, m

Greek

δ	boundary layer thickness, m
η	cooling efficiency
ξ	dimensionless centreline exit temperature
μ	dynamic viscosity, m^2s^{-1}
ρ	density, kg/m^3
τ	time constant, s
θ	temperature difference, °C

Subscripts

aw	adiabatic wall temperature
cl	centreline
$exit$	exit condition
$f\text{-}c$	film-cooling
g	gas
h	hole
i,n	counter
in	inlet
$init$	initial
mb	mixed-bulk
$surface$	local conditions at the surface
w	wall
∞	mainstream

REFERENCES

Bunker, R.S., Metzger, D.E., 1990, "Local Heat Transfer in Internally Cooled Turbine Airfoil Leading Edge Regions - Part 1: Impingement Cooling without Film Coolant Extraction," Journal of Turbomachinery - Transactions of the ASME, Vol. 112, No. 3, pp. 451-458.

Byerley, A.R., 1988, "Heat Transfer Near the Entrance to a Film Cooling Hole in a Gas Turbine Blade," D.Phil Thesis, Department of Engineering Science, University of Oxford.

Dailey, G.M., 2000, "Aero-thermal Performance of Internal Cooling Systems in Turbomachines: Design and Calculation Issues," VKI Lecture Series February 28th – March 3rd, 2000

Florschuetz, L.W., Metzger, D.E. and Truman, C.R., 1981,"Jet Array Impingement with Crossflow Correlation of Streamwise Resolved Flow and Heat Transfer Distributions," NASA Contractor report no. 3373.

Gillespie, D.R.H., "Turbine Rotor Blade Internal Cooling Studies," 1993, D.Phil. Transfer Report, University of Oxford.

Gillespie, D.R.H., 1996,"Intricate Internal Cooling Systems for Gas Turbine Blading," D.Phil. Thesis, University of Oxford.

Gillespie, D.R.H., Byerley, A.R., Wang, Z., Ireland, P.T., Jones, T.V., Kohler, S.T., 1996, "Detailed Measurements of Local Heat Transfer Coefficient in the Entrance to Normal and Inclined Film-Cooling Holes," Transactions of the ASME, Journal of Turbomachinery, 1996, Vol. 118, Nº2, pp.285-290.

Gillespie, D.R.H., Ireland, P.T., 1999,"Leading Edge Intersecting Hole Flow and Heat Transfer", OUEL Report 2199/99.

Halls, G.A., 1969, "Air Cooling of Turbine Blades and Vanes," Chapter 5, *Supersonic Turbojet Propulsion Systems and Components*, AGARDograph 120, pp. 262.

Ireland, P.T., 1987, "Internal Cooling of Turbine Blades," D.Phil Thesis, Department of Engineering Science, University of Oxford.

Kays, W.M., Crawford, M.E, 1980, *Convective Heat and Mass Transfer*, McGraw-Hill.

Mee, D.J., Ireland, P.T. and Bather, S., 1999,"Measurement of the Temperature Field Downstream of Simulated Leading-Edge Film-Cooling Holes, Experiments in Fluids, Vol. 27 No. 3 pp. 262-272.

Schultz, D.L., Jones, T.V., 1973, "Heat Transfer Measurements in Short Duration Hypersonic Facilities, AGARDograph No. 165.

Son, C.M., Gillespie D.R.H., Ireland, P.T., Dailey, G.M., 2000, "Heat Transfer Enhancement Strategy for an Impingement Cooling System", Proceedings of the 8th International Symposium on Transport Phenomena and Dynamics of Rotating Machinery, Vol. II, pp. 722-730

Son, C.M., Gillespie, D.R.H., Ireland, P.T., and Dailey, G.M., 2001, "Heat Transfer and Flow Characteristics of an Engine Representative Impingement Cooling System, Journal of Turbomachinery, Vol. 123, pp 154-160.

Son, C.M., Gillespie, D.R.H., Ireland, P.T., and Dailey, G.M., 2001, "Heat Transfer Characteristics of an Impingement Plate Used in a Turbine Vane Cooling System," accepted for presentation at ASME Turbo Expo 2001 June 4-7, 2001, New Orleans, Louisiana. ASME paper 2001-GT-154.

Suo, M., 1985, *Aerothermodynamics of Aircraft Engine Components*, AIAA Education Series, ed. Oates, G.C..

Taslim, M.E., Setayeshgar, L., Spring, S.D., 2000, "An Experimental Evaluation of Advanced Leading Edge Impingement Cooling Concepts", ASME TURBOEXPO 2000, Munich, Germany, ASME paper 2000-GT-222.

Van Treuren, K.,V., Wang, Z., Ireland, P.T., Jones, T.V., Kohler, S.J., 1993, "Detailed Measurements of Local Heat Transfer Coefficient and Adiabatic Wall Temperature Beneath an Array of Impinging Jets," Transactions of ASME, Journal of Turbomachinery, Vol.116., pp 369-374.

Wang, Z., Ireland, P.T., Jones, T.V., Davenport, R., 1994, "A Colour Image Processing System for Transient Liquid Crystal Heat Transfer Experiments," ASME paper 94-GT-290.

Paper Number: 25

Name of Discusser: H. Weyer, DLR Cologne

Question:
Obviously the Re-number in the experiment is fully represented. Can you please comment on the flow velocity level and it's effects on non-Re-dependent effects in impingement cooling. Which are the typical impulse ratios?

Answer:
The Mach number in both the engine and model are low (<< 0.3), and it may be assumed that there is no compressibility effect on heattransfer. Natural convection is insignificant compared to forced convection: Grashof number has not been matched. Once the engine representative Reynolds number has been modelled the ratio of cross-flow to jet-flow momentum, Gc/Gj, is also correctly modelled throughout the semi-confined channel.
It increases towards the exit. At the 1^{st} row Gc/Gj is close to zero rising to ≈ 0,35 at the channel exit. The introduction of additional cross-flow is the subject of further investigation currently underway at Oxford.

Name of Discusser: J. v. Wolfersdorf, Gas Turbines Development Baden Switzerl.

Question:
How did you determine the mass flow through the individual rows of holes especially for the case of varying hole diametery?

The Florshütz distributed flow model was used to predict the static pressure and flow distribution through each row of holes.
Despite the varying hole diameter and hence l/d the predicted static pressure at the exit of each hole matched well to values measured both on the side wall of the passage and individual cooling holes. Furthermore, stagnation point-heat-transfer coefficient data closely agreed with other workers measurements from the literature and showed no systematic scatter related to the hole diameter or the position in the array.

This page has been deliberately left blank

Page intentionnellement blanche